Electrodeposition of Cu-Zn-Sn coating in citrate medium

Yassine Salhi [1,*], Sghir Cherrouf [1], Jihane Tellal [1] and Mohammed Cherkaoui [1,2]

[1] Laboratory of Materials, Electrochemistry and Environment, Faculty of Science, Ibn Tofail University, Po Box 133-14050, Kenitra, Morocco

[2] National Higher School of Chemistry, Ibn Tofail University, Po Box 133-14050, Kenitra, Morocco

Abstract: The electrodeposition of Cu-Zn-Sn (CZT) coating at ambient temperature was investigated. The bath consists of metal salts $SnSO_4$, $ZnSO_4,7H_2O$ and $CuSO_4,5H_2O$ and sodium citrate ($NaC_6H_5Na_3O_7,2H_2O$) as a complexing agent. For precipitation, the pH is maintained at 5. The reducing of copper, tin and zinc through Cu_2HCit^{3-}, $Sncit^{2-}$ and $ZnHcit^{-}$ complexes respectively are confirmed by the presence of three cathodic peaks on the voltammograms realized on steel and ITO glass substrate. X-ray diffraction patterns revealed peaks corresponding to the phases: Cu-Zn cubic, Cu-Sn hexagonal and β-Sn tetragonal. The deposition rate is 35 μm/h. SEM observation and EDAX analysis showed that the coating consists of a uniform CZT layer of which composition is 55% copper, 20% zinc and 25% tin at -1.5V. A preliminary study showed a remarkable improvement in the corrosion resistance of CZT coated steel in comparison with bare steel.

Keywords: Cu-Zn-Sn (CZT) coating, citrate, electrodeposition, voltammetry, ITO, characterization, corrosion resistance.

1. Introduction

Cu-Zn-Sn (CZT) alloys coatings exhibit exciting characteristics: good corrosion resistance [1-5], excellent solderability [6-9], good ductility [10-12], no toxicity [13,14] and beautiful appearance and smooth morphology [15,16]. Thus, they are applied as a finish coat in many domains such as marine industry [1], the automobile industry [3,8], microelectronics [17,18], aeronautics [18], food industry [19]. Also, CZT deposits were used to prevent dezincification and improve the electrical properties of the Sn-Zn binary system by adding copper [20].

Furthermore, tin, zinc and copper are the main parts that constitute the layers used in photovoltaic cells when combined with sulfur or selenium to form quaternary deposits (Cu_2ZnSnS_4 (CZTS) and $Cu_2ZnSnSe_4$ (CZTSe)) [21-23].

Kesterite Cu_2ZnSnS_4 *(CZTS)* thin films are attracting much interest as an alternative system to *Cu(In, Ga)Se_2 (CIGS)* and *CdTe* thin films because *In, Ga* and *Te* are rare and expensive elements and the other reason is the toxicity of cadmium [24-29]. We also note that CZTS thin films offer excellent properties such as good mechanical properties and good absorption coefficient [28]. Besides, *CZTS* film contains Zn and Sn that are naturally abundant, very cheap materials to replace In and Ga. Beside, *CZTS* thin film has the same tetragonal structure as that of *CIGS* [29,30].

The major problem of co-deposition of metals is to bring their reduction potential closer. The addition of complexants in baths is a simple and effective solution. Thus, various complexing agents have been used in the case of the alloy CZT: tartrate [2], gluconate [10], citrate [4,13,20] and trisodium nitrilotriacetic [31]. In a previous Sn-Zn alloy electrodeposition study, we have chosen citrate to co-deposit tin and zinc because of the stability of the bath at a near-neutral pH in order to make industrial application easy [32].

We have opted for the same complexant in the case of the CZT ternary alloy coating electrodeposition. We have used the thermodynamic model of Kazimierczak H. et al. to determine the optimal pH range to obtain a stable electrolyte [4].

The CZT coating was carried out on copper and common steel substrates for the electrochemical study then on ITO glass in order to fabricate CZT precursor layers for a possible application in photovoltaic cells. On the other hand, morphology, composition, crystallographic study and corrosion resistance of CZT deposits were characterized by SEM, EDX, DRX and electrochemical impedance.

2. Experimental details

The electrolysis cell is a double-walled Pyrex cylinder with a volume of 100 ml. It is equipped with a Teflon lid with 5 apertures. Three of them allow the passage of electrodes necessary for electrochemical measurements: the working electrode, the counter electrode or auxiliary electrode and the reference electrode. The other two allow purging of the dissolved oxygen by nitrogen bubbling and temperature control. We have used steel, copper and ITO substrates with a surface area of $1 cm^2$ as working electrode, Pt plate as the counter while *SCESat* as the reference electrode to which potentials will be referred in the following.

Before the immersion test, the steel and copper substrates were abraded using emery paper up to 1200 grade, cleaned with ethanol, etched in 10% dilute sulfuric acid, washed with distilled water and dried finally. In the case of ITO glass, substrates were cleaned ultra-sonically in ethanol and dried before electrodeposition of CZT coating.

The electrolytes used are composed of tin sulfate, zinc sulfate, copper sulfate and sodium citrate as a complexing agent. The concentrations are given in Table 1. The pH was adjusted at 5 by sulfuric acid, and the temperature is set at $20 \pm 2°C$.

This formulation was chosen after some preliminary tests on the chemical stability in order to avoid the precipitation of the hydroxides.

The electrochemical measurements were carried out using Voltalab PGZ 100® (Potentiostat/Galvanostat) monitored by Voltamaster 4. The potential range was performed in between 0.5V and - 2V with a scan rate of 10mV/s and 25mV/s. The impedance studies were carried out in a frequency range of 100 kHz to 10mHz with the amplitude of $\pm$ 10mV. X-ray diffraction was performed by a PANalytical X'PERT3 POWDER diffractometer with Cu Kα1 radiation.

The E_{corr} corrosion potential and the I_{corr} corrosion current was performed using nonlinear regression using the Origin 6 software. The morphology of the coatings was analyzed by the FEI Quanta 200 scanning electron microscope. The chemical composition of the CZT deposit elements was determined by EDX. The mass of the deposit was determined by an analytical balance with an accuracy of 0.1mg.

Table 1. Composition of the deposits baths

Electrolytes	$SnSO_4$ (mole /L)	$ZnSO4, 7 H_2O$ (mole /L)	$CuSO_4, 5 H_2O$ (mole /L)	$NaC_6H_5Na_3O_7$, $2H_2O$ (mole /L)	pH
1	-	-	-	0.5	5
2	-	-	0.08	0.5	5
3	0.14	-	-	0.5	5
4	-	0.22	-	0.5	5
5	0.14	-	0.08	0.5	5
6	-	0.22	0.08	0.5	5
7	0.14	0.22	-	0.5	5
8	0.14	0.22	0.08	0.5	5
9	0.028	0.044	0.016	0.1	5

3. Results and discussion

3.1. Baths stability

The major problem in the electroplating of CZT ternary alloys is the preparation of a stable electrolyte. Preventing the precipitation of tin (II), zinc (II) and copper (II) hydroxides in these baths is essential.

Thus, the addition of citrate in electrodeposition baths is of great interest because it forms aqueous and electroactive complexes with Sn (II), Zn (II) and Cu (II). We used the *H. Kazimierczak et al.* model to determine the areas of the predominance of Cu-cit, Sn-cit and Zn-cit species as a function of sodium citrate concentration and pH of the solution as it is shown in Figs 1, 2 and 3. Thus, we observe that the existence of the electroactive complexes: $SnCit^{2-}$, $ZnHCit^-$ and $Cu_2HCit_2^{3-}$ and $Cu_2Cit_2^{4-}$ are around pH = 5.
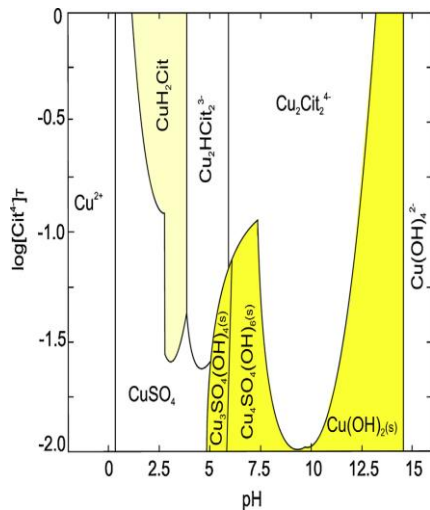
Figure 1. Predominance diagram of Cu (II) species [20]
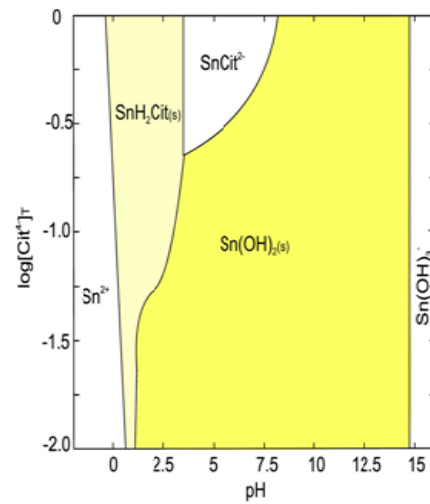
Figure 2. Predominance diagram of Sn (II) species [20]
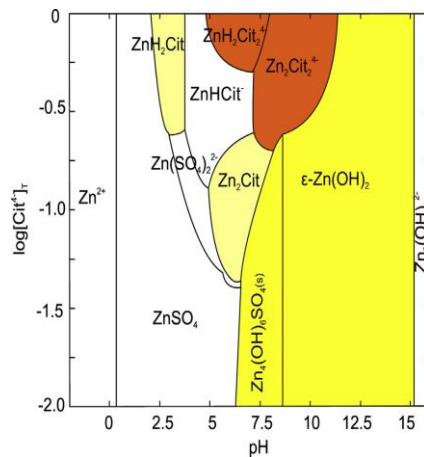
Figure 3. Predominance diagram of Zn (II) species [20]

3.2. Voltammetric study
3.2.1. Citrate bath
Fig.4 shows the voltammogram realized in the electrolyte (1) containing the only citrate on a copper substrate.
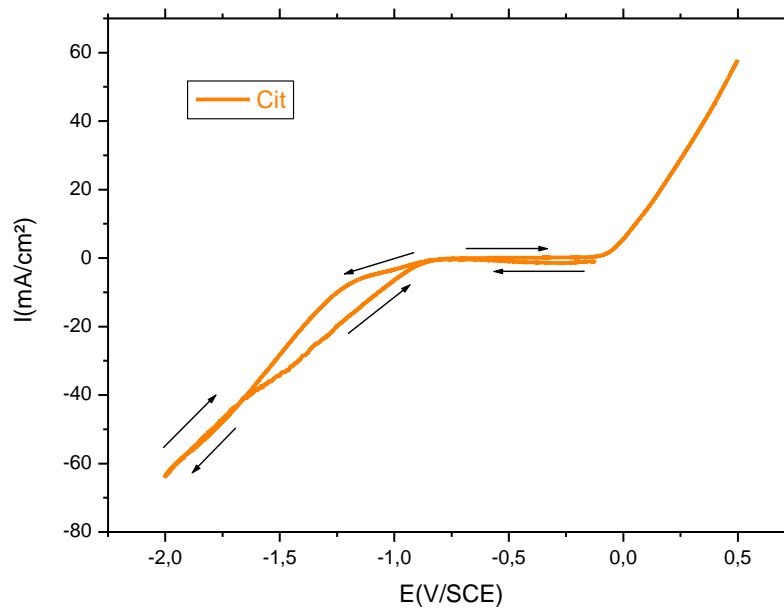
Fig.4 Cyclic voltammogram on a copper substrate in a solution containing only citrate (electrolyte 1) at v = 10mV/s

We observed a cathodic current from -1.05V related to the process of hydrogen evolution via the reduction of the protonated form H_2cit^{2-} according to the reaction:

$$2H_2cit^{2-} + 2e^- \rightarrow H_2 + 2Hcit^{3-} \qquad (1)$$

An identical result was obtained on steel in a previous study [32].

3.2.2. Citrate-cupric ion bath

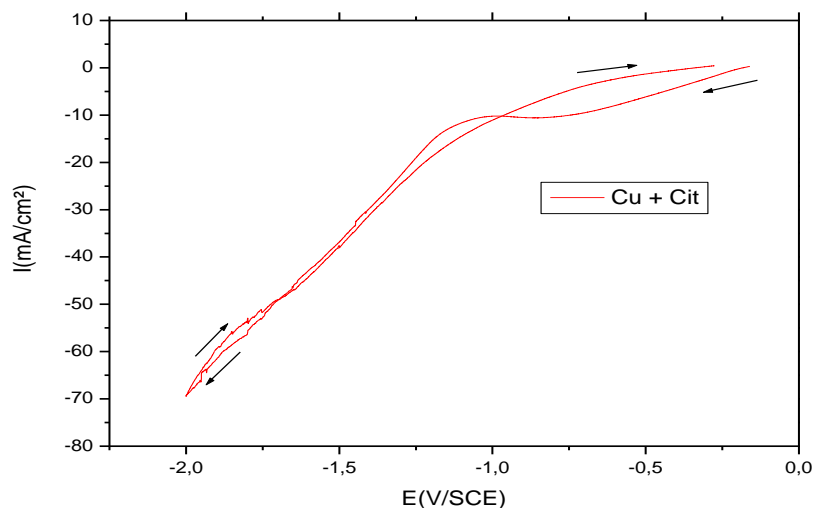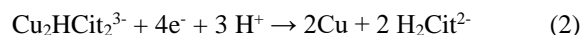Fig.5 shows the voltammogram realized in the solution containing cupric ions and citrate. A wave of reduction appearing at -0.1V would be attributed to the reduction of $Cu_2HCit_2^{3-}$ cupric complex according to the reaction:

$$Cu_2HCit_2^{3-} + 4e^- + 3 H^+ \rightarrow 2Cu + 2 H_2Cit^{2-} \qquad (2)$$

A slight plateau of cathodic current density is observed due to the diffusion of cupric ions and then a rapid increase in the current density related to the evolution process of hydrogen.

Fig.5 Cyclic voltammogram on a copper substrate in a solution containing citrate and copper (electrolyte2) at v = 25mV/s

3.2.3. Citrate-stannous ion bath

Fig.6 shows the voltammogram realized in a solution containing citrate and stannous ions. The reduction of Sn (II) via the hydrogenated Sn-citrate complex starts at -0.75V according to the reaction :
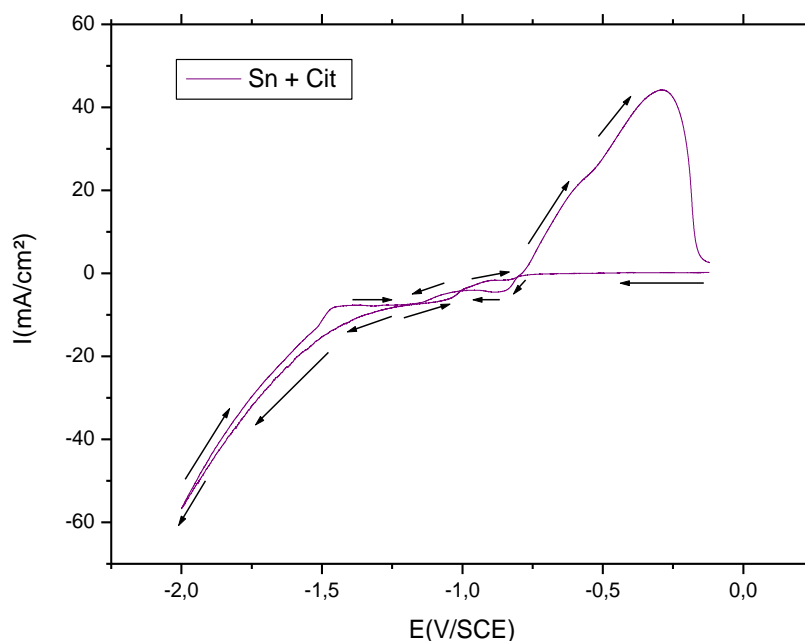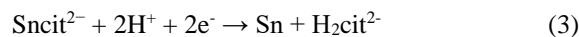
$$Sncit^{2-} + 2H^+ + 2e^- \rightarrow Sn + H_2cit^{2-} \qquad (3)$$

Fig.6 Cyclic voltammogram on a copper substrate in a solution containing citrate and tin (electrolyte3) at 25mV/s

This potential is shifted by 100 mV compared to the study carried out on steel [32]. A plateau of cathodic current density attributed to the diffusion of stannous ions and a process of evolution of hydrogen from the protonated form H_2cit^{2-} are observed.

3.2.4. Citrate-zinc ion bath

Fig.7 shows the voltammogram obtained in a solution containing citrate and zinc ions. A cathodic current appears around -1V linked to the process of hydrogen evolution via the reduction of the protonated form H_2cit^{2-}. Then, we observe a decrease in the current density from -1.6V related to the reduction of hydrogenated Zn-citrate complexes:

$$ZnHcit^- + H^+ + 2e^- \rightarrow Zn + H_2cit^{2-} \qquad (4)$$
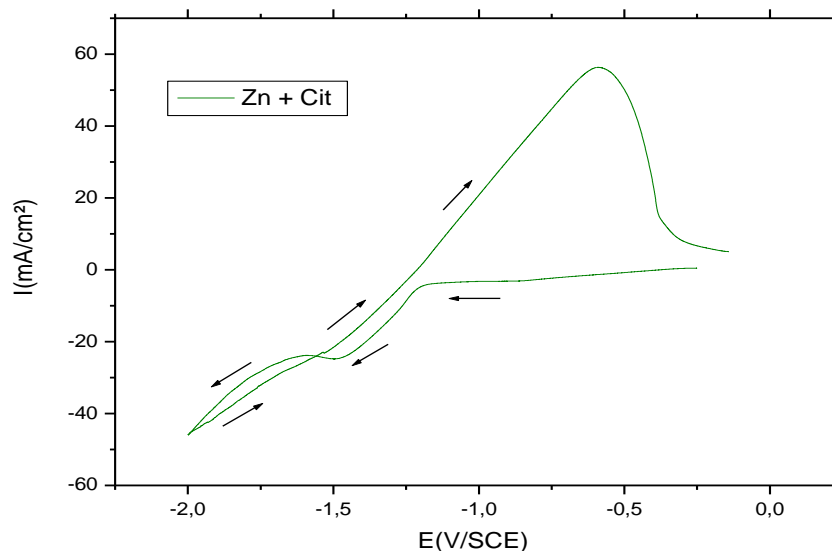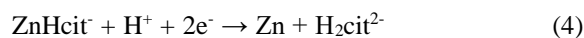

Figure 7. Cyclic voltammogram on the copper substrate in a solution containing citrate and zinc (electrolyte 4) at 25mV/s

3.2.5. Citrate-cupric and stannous ion bath

Fig.8 shows the voltammogram obtained in the electrolyte containing citrate and cupric and stannous ions. It presents three reduction waves of $Cu_2HCit_2^{3-}$, $Sncit^{2-}$ and H_2Cit^{2-} that appear at potentials practically similar to those obtained in the baths containing respectively citrate-cupric ions, citrate-stannous ions and citrate. On the other hand, we notice that the intensity of the reduction peak of the stannous ions is high. Indeed, the X-ray diffraction patterns of a deposit made at a potential -0.9V show two phases tetragonal β-Sn and Cu_6Sn_5 (Fig.9)
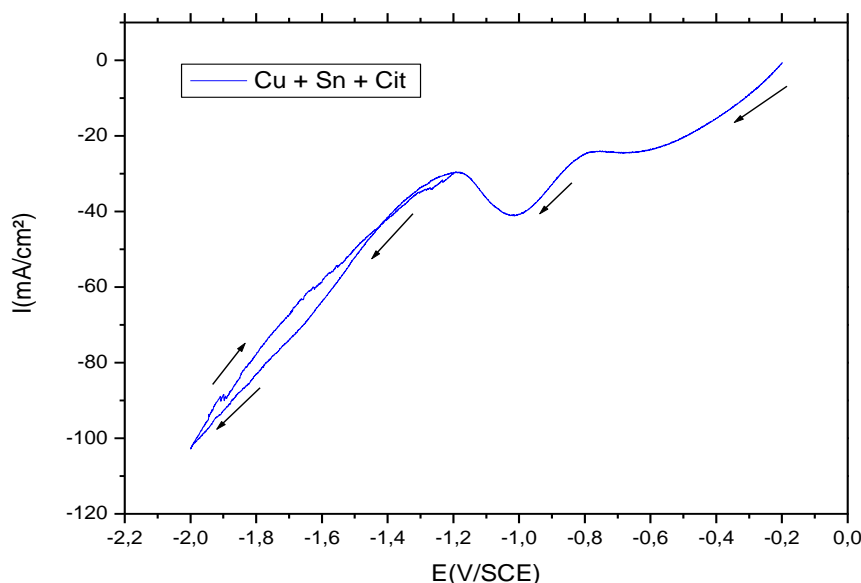

Figure 8. Cyclic voltammogram on the copper substrate in a solution containing citrate, tin and copper (electrolyte 5) at 25mV/s.
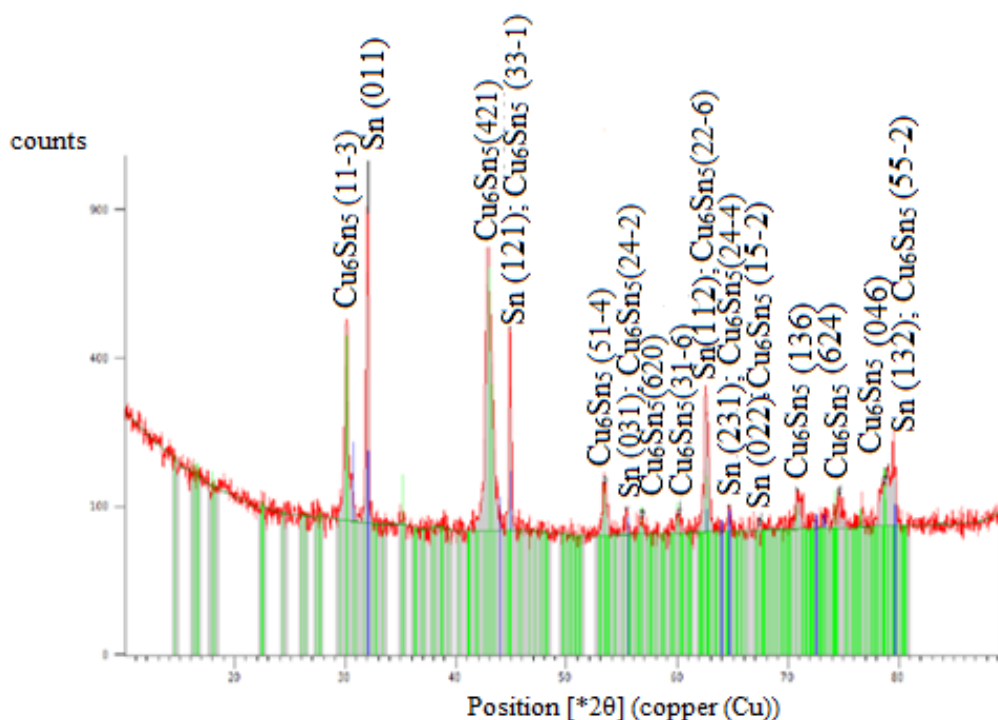
Figure 9. X-ray diffraction patterns for a deposit obtained on steel at E = -0.9 V in a solution containing citrate, tin and copper (electrolyte 5)

3.2.6. Citrate-cupric ion bath and zinc ions

Fig.10 shows the voltammogram realized in a citrate solution containing copper and zinc ions. Copper reduction begins at a potential of -0.1V as expected. The cathodic current around -1V would be related to the process of hydrogen evolution via the reduction of the protonated form H_2Cit^{2-}. Then, we see a substantial increase in the current density due to the zinc electrodeposition via the hydrogenated Zn-citrate complexes.
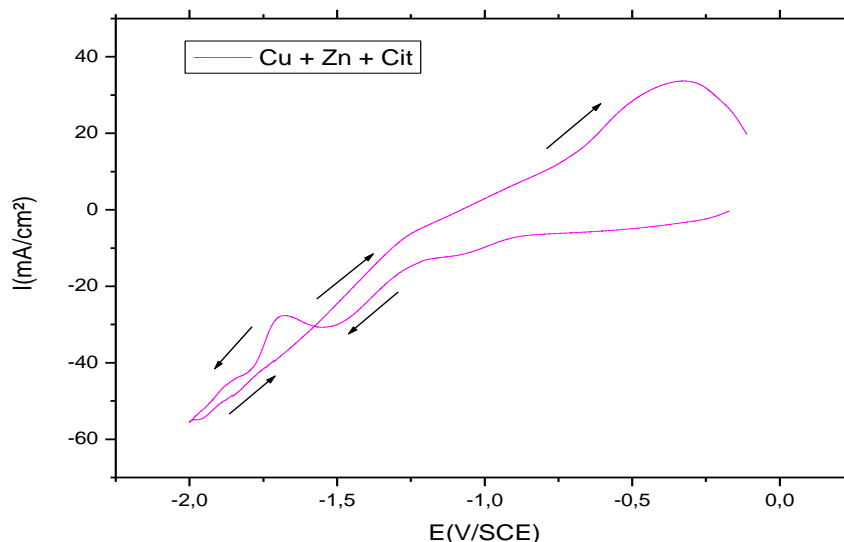

Fig.10 Cyclic voltammogram on the copper substrate in a solution containing citrate, copper and zinc (electrolyte 6) at 25mV/s

3.2.7. Citrate-tin-zinc bath

Fig.11 shows the voltammogram realized in a citrate solution containing tin and zinc. The simultaneous presence of tin and zinc does not influence the voltammetric response. The reduction waves of tin via $Sncit^{2-}$ and zinc via $ZnHcit^-$ appear almost at the same potential as in the baths containing respectively citrate-stannous and citrate-zinc ions.
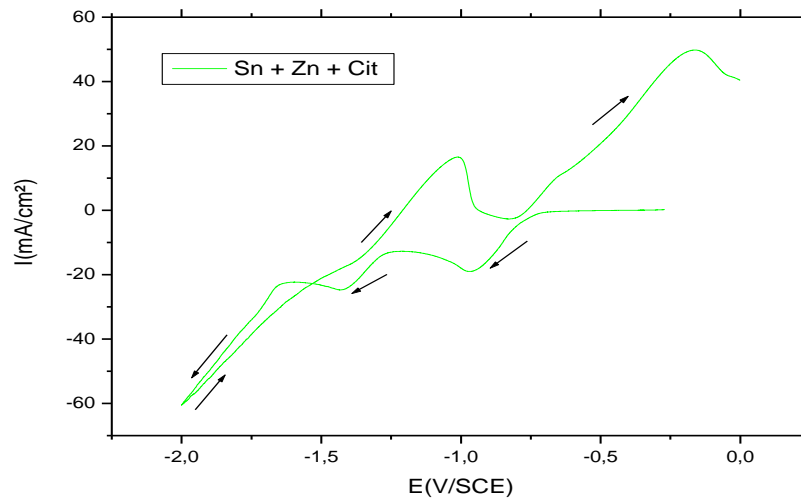
Fig.11 Cyclic voltammogram on a copper substrate in a solution containing citrate, tin and zinc (electrolyte 7) at 10mV/s

3.2.8. Citrate-copper-zinc-tin bath

Figs 12 and 13 show the voltammograms realized in a solution containing citrate and copper, tin and zinc ions and on copper and ITO glass substrates.
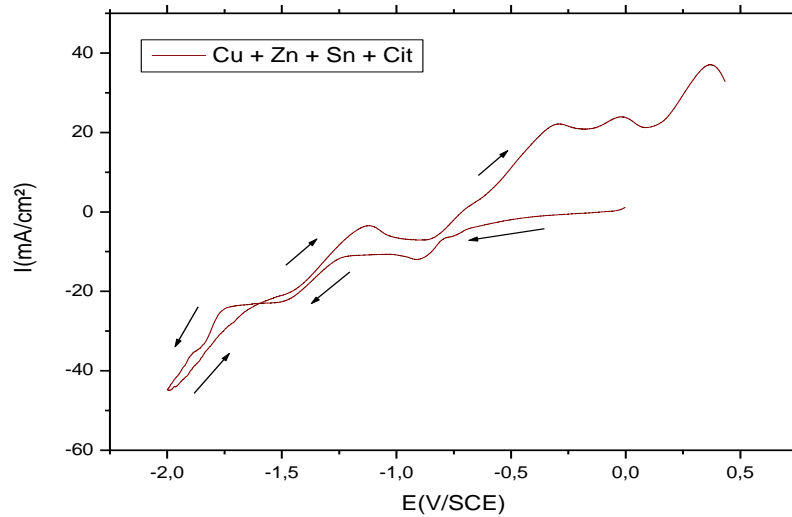

Fig.12 Cyclic voltammogram on a copper substrate in a solution containing citrate, tin, zinc and copper (electrolyte 8) at 10 mV/s
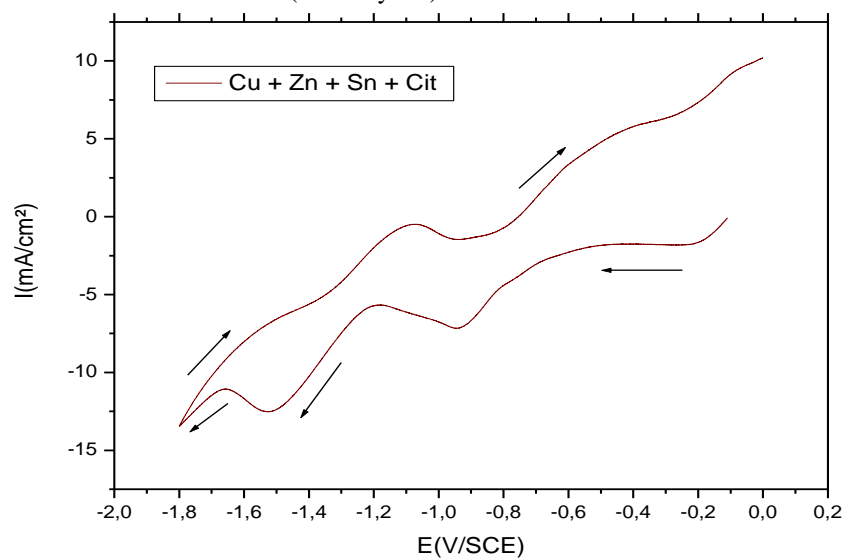

Fig.13 Cyclic voltammogram on ITO glass substrate in a solution containing citrate, tin, zinc and copper (electrolyte 9) at 25mV/s

We observe in both cases four cathodic waves corresponding respectively to the reduction of the species $Cu_2HCit_2^{3-}$, $Sncit^{2-}$, H_2Cit^{2-} and $ZnHcit^-$ appearing at the same potentials as for the electrolytes containing each metal ion with citrate. Indeed, the deposit is ternary and consists of copper, tin and zinc. The X-ray diffraction patterns of CZT coating electrodeposited at a current density of $-22.5mA/cm^2$ ($-1.5V$) on steel show three phases: tetragonal β-Sn and Cu_6Sn_5 and $Cu_{18.20}$ $Zn_{33.80}$ (Fig.14). During the reverse scan, we observe three anodic waves corresponding to the oxidation of zinc, tin and copper as observed by authors [20].
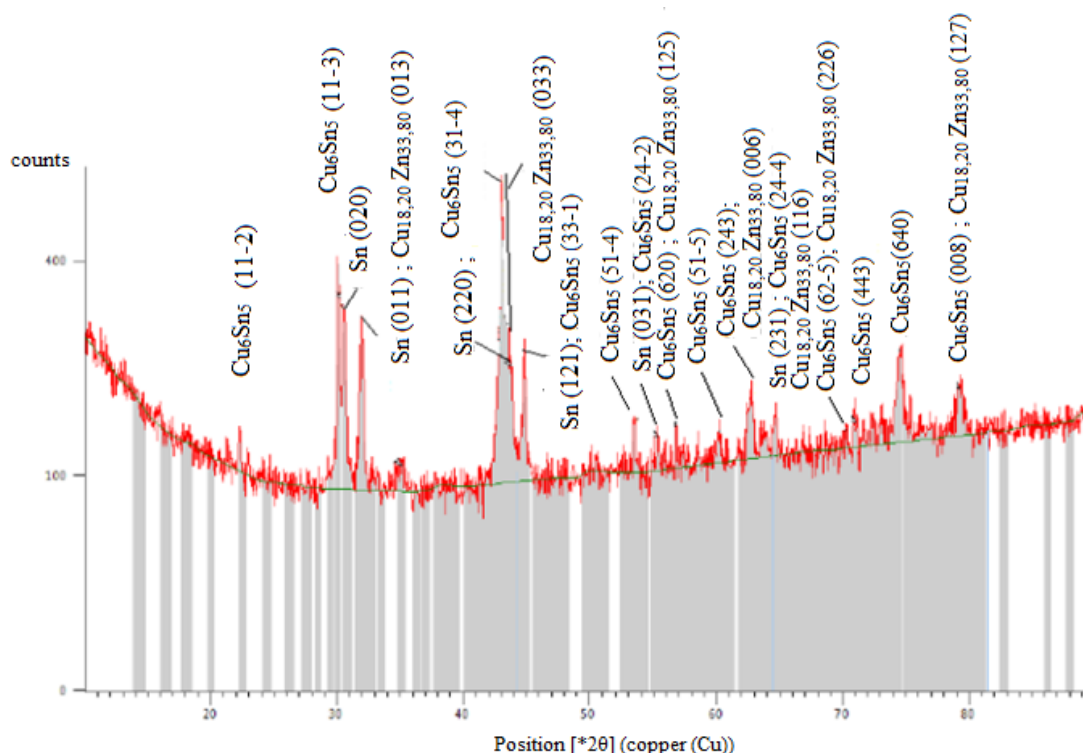

Figure 14. X-ray diffraction patterns for CZT coating electrodeposited on steel at $-22.5mA/cm^2$ (electrolyte 8)

3.3. Characterization of CZT coating electrodeposited on steel
3.3.1. Rate and deposition efficiency
The deposition rate V was determined by the following formula:

$$V(\mu m/h) = e / t$$

e: coating thickness (μm), t: deposition time (h)
For an electrodeposited coating, at E = -1.5V (I = $-22.5mA/cm^2$), the thickness was calculated according to the relation:

$$e(\mu m) = \frac{mf - mi}{\rho.S} . 10^{-4} = \frac{\Delta m}{\rho.S} . 10^{-4}$$

$mf(g)$: final weigh of the sample, $mi\ (g)$: initial weigh of the sample, Δm_{exp} (g): experimentally deposited mass, $_\varrho$(g/cm³): density of deposit =

$$0.55\rho(Cu) + 0.25\rho(Sn) + 0.20\rho(Zn)$$

[$\rho(Cu)$ =8.9g/cm³, $\rho(Sn)$=7.28g/cm³, $\rho(Zn) = $ 7.14g/cm³], S (cm²): substrat surface (1cm²).

Moreover, according to Faraday's law, the theoretical deposited mass md is obtained by the following expression:

$$m_{th} = I . t . M_d / Z . F$$

I: deposition current, t: deposition time (s), **M_d**: molar mass of the deposit = 0.55 M_{Cu} (63.55 g/mol) + 0.25M_{Sn} (118.7g/mol) + M_{Zn} (65.4g/mol), **F**: 96500C, **Z**: number of transferred electron.

The deposition efficiency $R_d = \Delta m / m_{th}$

The values of mass variation, thickness, rate and deposition efficiency are summarized in Table 2.

Table 2. Characteristics of the CZT coating.

Δm_{exp}	m_{th}	t	ρ	e	v	R_d
0.0071g	0.0082g	0.25 h	8.14g/cm³	8.7 µm	34.8µm/h	0.87

We note that the deposition rate is relatively high, and the deposition efficiency R_d is less than 1. This is attributed to the fact that part of the applied current is consumed by the reduction of hydrogen. The same procedure was carried out in the case of a coating electrodeposited on ITO glass; the deposition rate is twice slower.

3.3.2. Morphology

Fig.15 shows SEM image of CZT coating obtained at E = -1.5V (I = -22.5mA/cm^2) on steel. We observe granular and adherent coating without cracks, but it presents some pores and irregularities. It consists of 55 at% copper, 25 at% tin and 20 at% zinc (Fig.16).
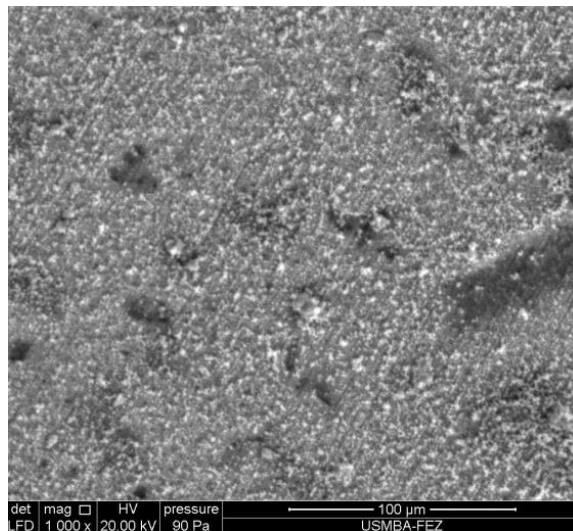

Figure 15. SEM images of CZT coating obtained on steel substrate (electrolyte 8) at E = -1.5V (I = -22.5mA/cm^2)
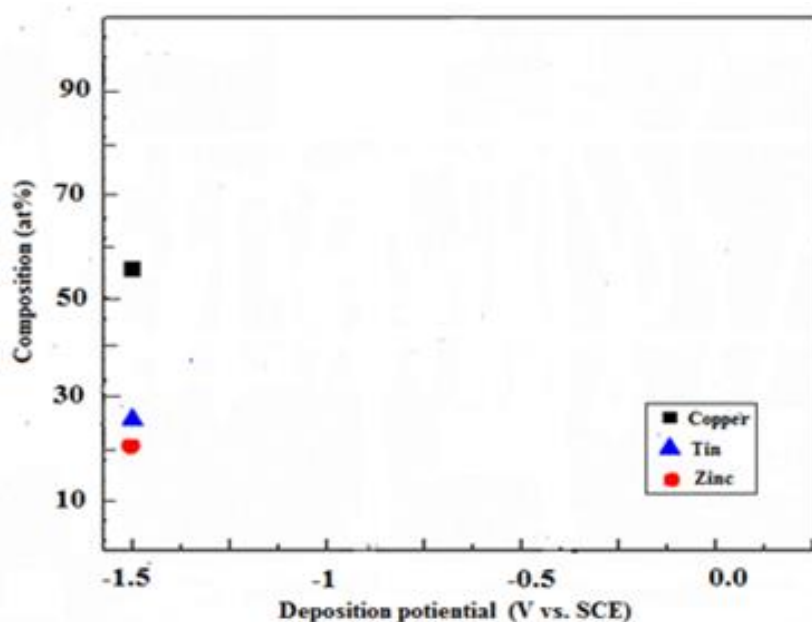

Fig.16 Chemical composition analysis of the electrodeposited CZT coating at E = -1.5V (I = -22.5mA/cm²) by EDAX

3.3.3. Corrosion resistance

The corrosion resistance of the CZT coating electrodeposited at -22.5mA/cm² in NaCl (3%) was characterized by the determination of the I_{corr} corrosion current and the E_{corr} corrosion potential using polarization curves and electrochemical impedance polarization resistance.

Fig.17 shows the polarization curves for steel and CZT coated steel with a thickness of 8.7μm. The electrochemical parameters are reported in Table 3. We note that the E_{corr} corrosion potential of CZT coated steel is much more anodic than that of bare steel and that I_{corr} corrosion current significantly decreases in the case of the ternary coating.
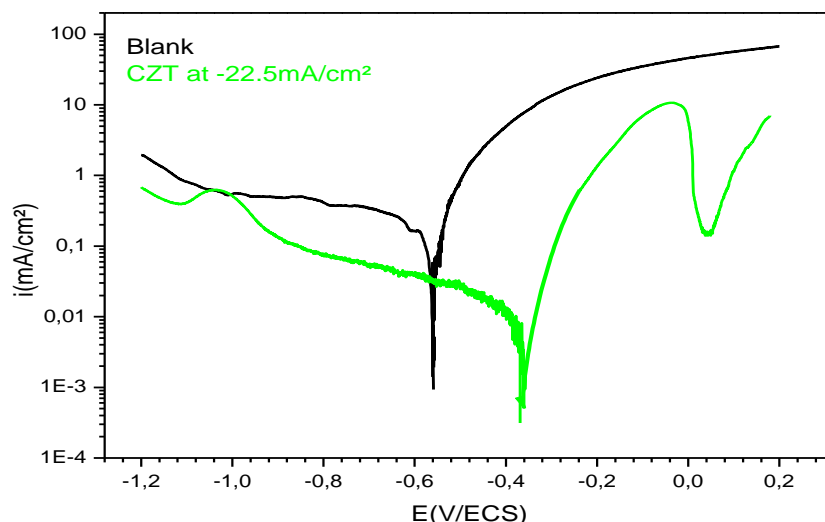
Figure 17. I = (E) curves for bare steel (Blank) and CZT coated steel at -22.5mA/cm² (-1.5V) in NaCl 3%

Table 3. Electrochemical parameters of steel and CZT coated steel.

	E_{corr} (mV/SCE)	I_{corr} (µA/cm²)	β_a (mV/dec)	β_c (mV/dec)
Bare steel	-560	280	121	-121
CZT coated steel at -22.5mA/cm²	-360	2.53	73	51

Fig.18 shows the Nyquist impedance diagram of bare steel and CZT coated steel made in 3% NaCl. The Nyquist diagram of bare steel is practically a small semicircle whereas that of CZT coated steel is a big one. The electrochemical impedance parameters are reported in Table 4. We note that the polarization resistance Rp is significantly higher for CZT coated steel. Thus, the polarization and electrochemical impedance measurements show that the CZT coating provides excellent protection against corrosion.
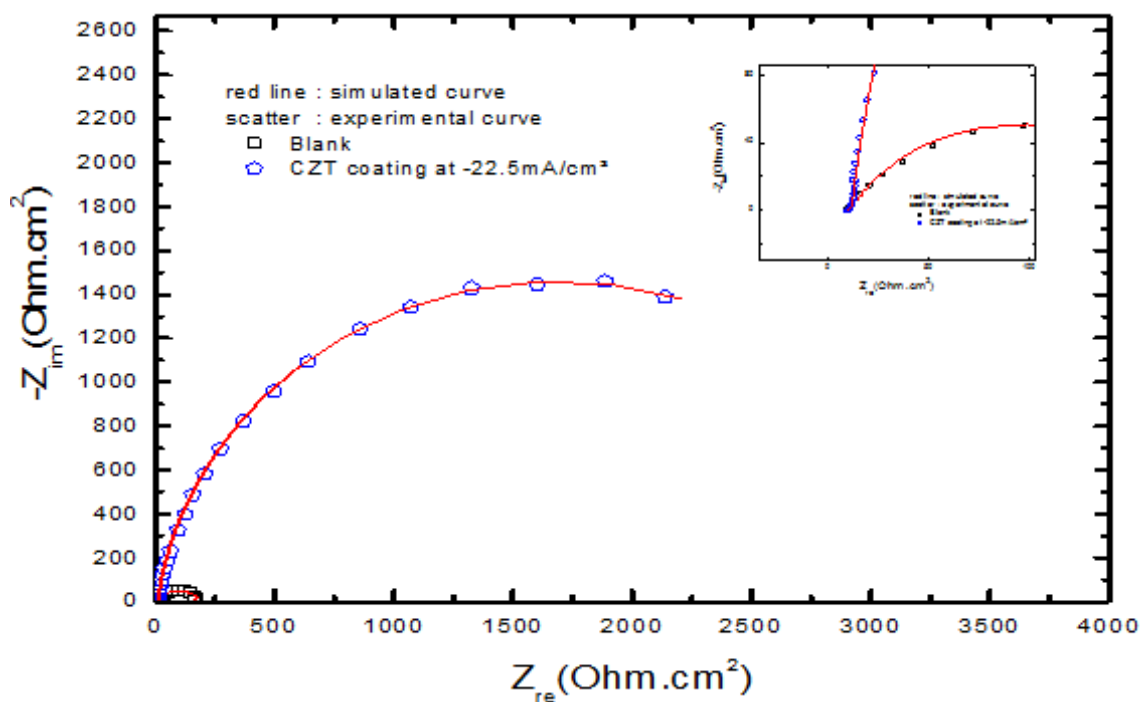

Figure 18. Nyquist diagram for bare steel (Blank) and ternary CZT coating at -22.5mA/cm²

Table 4. Electrochemical impedance parameters of bare steel and CZT coated steel.

	Rs (Ω cm²)	Rf (Ω cm²)	n	Qf (µF/cm²)	n	Qct (µF/cm²)	Rct (Ω cm²)	Rp (Ω cm²)
Bare steel (Blank)	10	--	--	--	1	201	175	165
CZT coated steel at -22.5mA/cm²	9.51	4.93	0.8474	1375	1	1231	3383	3378.42

4. Conclusion

In this study, the deposit of CZT was developed at ambient temperature on a steel and ITO substrates with citrate as a complexing agent. At a potential of -1.5V (I=-22.5mA.cm⁻²), the deposition rate of the coating is 34.8 µm/h on steel whereas on ITO glass is twice slower. Electrochemical investigations showed that copper, tin and zinc were reduced via Cu-citrate ($Cu_2HCit_2^{3-}$), Sn-citrate ($Sncit^{2-}$) and Zn-citrate ($ZnHcit^-$) complexes, respectively. The SEM observation revealed a granular and adherent coating without cracks, but some pores and irregularities were observed. The coating composition at -1,05V consists of 55 at% copper, 25 at% tin and 20 at% zinc according to EDAX analysis. The X-ray diffraction patterns of CZT coating electrodeposited at a current density of -22.5 mA/cm² (-1.5V) on steel show three phases: tetragonal β-Sn and Cu_6Sn_5 and $Cu_{18.20}$ $Zn_{33.80}$. There is also a remarkable improvement in the corrosion resistance of the steel coated by the CZT deposit compared to bare steel. Indeed, the polarization resistance Rp measured by electrochemical impedance is significantly higher for the coated steel.

References

1- E. Budman, D. Stevens, Tin-Zinc plating, Trans. Inst. Met. Finish., **1998**, 76(3), B34.

2- E. Guaus, J. Torrent-Burgue´s, Tin–zinc electrodeposition from sulphate–tartrate baths, J. of Electroanal. Chem., **2005**, 575, 301-309.

3- S. Dubent, M.L.A.D. Mertens, M. Saurat, Electrodeposition, characterization and corrosion behaviour of tin-20 wt.% zinc coatings electroplated from a non-cyanide alkaline bath, Mat. Chem. Phys., **2010**, 120, 371-380.

4- H. Kazimierczak, P. Ozga, Electrodeposition of Sn–Zn and Sn–Zn–Mo layers from citrate solutions, Surf. Sci., **2013**, 607, 33-38.

5- J. Zhang, C. Gu, J. Tu, Potentiodynamical deposition and corrosion behavior of thin Zn-Sn coatings with a layered structure and varied composition from deep eutectic solvent, Surf. Coat. Tech., **2017**, 320, 640-647.

6- S.J. Blunden, A.J. Killmeyer, Sn-Zn alloy electroplates outperform cadmium deposits, Adv. Mater. Processes, **1991**, 140(6), 37-39.

7- European Patent Plating bath and method for electroplating tin-zinc alloys, EP 1 201 789 B9, **2002**, 1-17.

8- E. Budman, M. McCoy, Tin-Zinc plating, Met. Finish., **1995**, 93 (9), 10-11.

9- M. Kiajima, T. Shono, Development of Sn-Zn-Al Lead-Free Solder Alloys, FUJITSU Sci. Tech. J., **2005**, 41(2), 225-235.

10-E. Guaus, J. Torrent-Burgue´s, Tin-zinc electrodeposition from sulphate-/gluconate baths, J. Electroanal. Chem., **2003**, 549, 25-36.

11-S. Dubent, M. De Petris-Wery, M. Saurat, H.F. Ayedi, Composition control of tin–zinc electrodeposits through means of experimental strategies, Mat. Chem. Phys., **2007**, 104, 146-152.

12-C. Zanella, S. Xing, F. Deflorian, Effect of electrodeposition parameters on chemical and morphological characteristics of Cu–Sn coatings from a methanesulfonic acid electrolyte, Surf. Coat. Tech., **2013**, 236, 394-399.

13-H. Kazimierczak, P. Ozga, A. Jałowiec, R. Kowalik, Tin–zinc alloy electrodeposition from aqueous citrate baths, Surf. Coat. Tech., **2014**, 240, 311-319.

14-W. Zhang, J. Guebey, M. Toben, K. Weitershaus, Neuer Hochgeschwindigkeitselektrolyt für die galvanise Abscheidung von glänzenden Reinzinnschichten bei erhöhten Betriebstemperaturen, Luzern/Schweiz, **2011**, 520-528.

15-A. Sharma, S. Bhattacharya, S. Das, K. Das, Influence of current density on surface morphology and properties of pulse plated tin films from citrate electrolyte, Appl. Surf. Sci., **2014**, 290, 373-380.

16-J.F. Huang, I.W. Sun, Electrochemical Studies of Tin in Zinc Chloride-1-ethyl-3-methylimidazolium Chloride Ionic Liquids, J. Electroch. Soc., **2003**, 150 (6), 299-306.

17-S. Ho Kee, W.J. Kim, J.P. Jung, Reflection characteristics of electroless deposited Sn-3.5Ag for LED lead frames, Surf. Coat. Tech., **2013**, 235, 778-783.

18-W.X. Zhang, Z.H. Jiang, G.Y. Li, Q. Jiang, J.S. Lian, Electroless Ni–Sn–P coating on AZ91D magnesium alloy and its corrosion resistance, Surf. Coat. Tech., **2008**, 202, 2570-2576.

19-E. Rudnik, G. Włoch, Studies on the electrodeposition of tin from acidic chloride–gluconate solutions, Appl. Surf. Sci., **2013**, 265, 839-849.

20- M. Slupska, P. Ozga, Electrodeposition of Sn-Zn-Cu alloys from citrate solutions, Electrochimica Acta, **2014**, 141, 149–160.

21-R. Lechner, S. Jost, J. Palm, M. Gowtham, F. Sorin, B. Louis, H. Yoo, R.A. Wibowo, R. Hock, $Cu_2ZnSn(S, Se)_4$ solar cells processed by rapid thermal processing of stacked elemental layer precursors, Thin Solid Films, **2012**, 535, 5-9.

22-J. Iljina, O. Volobujeva, T. Raadik, N. Revathi, J. Raudoja, M. Loorits, R. Traksmaa, E. Mellikov, Selenisation of sequentially electrodeposited Cu–Zn and Sn precursor layers, Thin Solid Films, **2013**, 535,14-17.

23- G. Banerjee, S. Das, S. Ghoch, Optical Properties of Cu_2ZnSnS_4 (CZTS) Made By SILAR Method, Materialstoday: PROCEEDINGS, **2019**, 18 Part 2, 494-500.

24-R.N. Bhattacharya, J.Y. Kim, Cu-Zn-Sn-S Thin Films from Electrodeposited Metallic Precursor Layers, The Open Surface Science Journal, **2012**, 4, 19-24.

25-Z. Chea, L. Han, L. Wan, C. Zhang, H. Niu, J. Xu, $Cu_2ZnSnSe_4$ thin films prepared by selenization of co-electroplated Cu–Zn–Sn precursors, Applied Surface Science, **2011**, 257, 8490-8492.

26-Studies of Cu_2ZnSnS_4 films prepared by sulfurisation of electrodeposited precursors by Jonathan James Scragg, University of Bath, Department of Chemistry, **2010**, 1-244.

27-Elektrochemische Legierungsabscheidung zur Herstellung von Cu_2ZnSnS_4 Dünnschichtsolarzellen von Holger H. Kühnlein aus Breitengüßbach, Dresden Universität, **2007**, 1-127.

28-M. Valdes, M. Modibedi, M. Mathe, T. Hilliec, M. Vazqueza, Electrodeposited Cu_2ZnSnS_4 thin films, Electrochimica Acta, **2014**, 128, 393–399.

29-R. Juskenas , S. Kanapeckaite, V. Karpaviciene, Z. Mockus, V. Pakstas, A. Selskiene, R. Giraitis, G. Niaura, A two-step approach for electrochemical deposition of Cu–Zn–Sn and Se precursors for CZTSe solar cells, Solar Energy Materials & Solar Cells, **2012**, 101, 277–282.

30-M.S. Kumar, S.P. Madhusudanan, S.K. Batabyal, Substitution of Zn in Earth Abundant $Cu_2ZnSn(S, Se)_4$ based thin-film solar cells – A status review, Solar Energy Materials and Solar Cells, **2018**, 185, 287-299.

31-M.F. de Carvalho, I.A. Carlos, Microstructural characterization of Cu-Sn-Zn electrodeposits produced potentiostatically from acid baths based on trisodium nitrilotriacetic, Journal of Electroanalytical Chemistry, **2018**, 823, 737-746.

32-Y. Salhi, S. Cherrouf, M. Cherkaoui, K. Abdelouahdi, Electrodeposition of nanostructured Sn–Zn coatings, Applied Surface Science, **2016**, 367, 64-69.